Intracavity Optogalvanic Spectroscopy applied to Radiocarbon Detection

by

Junming Liu

A Dissertation submitted to the

Graduate School-Newark

Rutgers, The State University of New Jersey

in partial fulfillment of the requirements

for the degree of

Master of Science

Graduate Program in Applied Physics

written under the direction of

Daniel Murnick

_____Daniel Murnick_____

_____Martin Schaden_____

_____Wu Zhen_____

_____

Newark, New Jersey

October, 2015

ABSTRACT OF THE DISSERTATION

Intracavity Optogalvanic Spectroscopy applied to

Radiocarbon Detection

By Junming Liu

Dissertation Director:

Daniel Murnick

Radiocarbon is extremely useful for archeological dating as well as for clinical, laboratory and atmospheric tracer applications. In this thesis, we report a new physical description of the ICOGS system process of radiocarbon optogalvanic signal extraction and analysis. To be specific, we first describe the fundamental theory of the Optogalvanic effect. Based on a set of 4-energy level rate equations for N_2 buffer gas and a set of 2-energy level for CO_2 sample gas, we simulate the N_2 and \$$CO_2$ ICOGS OG signals. Moreover, according to the phase difference from our simulation and experiment observation, we propose three methods (1.Vector Phase and Amplitude fitting, 2.Differential Method and 3.Vector Decomposition Method) to separate CO_2 OG signal from N_2 OG signal. Experimental results demonstrate our quantitative radiocarbon detection near 10 zeptomole 14C levels in 10 Mg samples.

Acknowledgement

I would never have been able to finish my dissertation without the guidance of my advisor, help from friends, and support from my family and wife. I would like to express my deepest gratitude to my advisor, Dr. Daniel Murnick, for his excellent guidance, caring and patience. I would like to thank Dr. Tulu, who as a good friend, was always willing to help and give his best suggestions. It would have been a lonely lab without him. Many thanks to Mark in the laboratory of Dr. Daniel for helping me with the facilities from the field. My research would not have been possible without their helps.

Lists of Tables

List of Figures

0.1 Introduction

Carbon 14 (radiocarbon14C) is an ideal organic tracer with an extremely low natural abundance in living systems, near 1 ppt, and a long half-life, 5730 years, making it extremely useful for archeological dating as well as for clinical, laboratory and atmospheric tracer applications. Until recently, almost all14C quantitation technologies are based on Scintillation detection of low energy beta particles emitted from14C decay. However, although Scintillation detection has high sensitivity for beta detection with good specificity, its sensitivity for14C detection is low since there is only one disintegration per minute for every 4.35 billion14C present in a sample. For an extremely large sample consisting of purified scintillation fluid (~ 5 Mg carbon), using well shielded, low background scintillation detectors, impressively low14C concentrations (~ 2×10^{-18}, or 10 pg) have been reported.[1]. However, carbon dating and tracer experiments often involve sub-mg samples that require higher sensitivity and faster response than s possible with beta counting. In the drug development community, there is great interest in using non-therapeutic microdoses of14C-labeled drugs to obtain pharmacokinetic information of new drug entities. Because of the small sample mass available for measurement, these studies require much higher analysis sensitivity and throughout than is possible with scintillation counting. [13]. In addition, environmental monitoring of biospheric radiocarbon, important for separating biogenic based CO2from fossil fuel based requires continuous monitoring at multiple sites. Accelerator Mass Spectroscopy (AMS), an atom counting method first developed to extend carbon dating to smaller and older

samples, has now become the standard method for14C analysis in precise dating, forensic and bioanalytical tracer studies[25, 20]. Total carbon content and14C detection limit are correlated. The AMS detection limit is near 10 zeptomole14C for samples of order 1 mg total carbon with an increase to ∼ 100 zeptomole14C with samples as small as 100 µgC. Limitations to wider use of AMS, especially for bioanalytical studies.

0.2 ICOGS Theory

ICOGS evolved from the laser assisted ratio analyzer (LARA) technique[19, 18, 17] and is based on the existence of large isotope shifts in molecular spectra, the use of single mode fixed frequency isotopic lasers and sensitive detection via the laser optogalvanic effect (OGE). Commercially available sealed CO2lasers filled with a14CO2laser mixture provides the required specificity to a unique transition in the14CO2molecule, typically the P(20) laser transition at 11.767726 microns[4]. This unique transition with an intrinsic linewidth less than 100Hz was known in the 1980s, and the ICOGS measuremnts shown here could have been carried out 30 years ago with existing technology. In contrast, the SCAR work which was also anticipated in the 1980s was not implemented until 2011 because new highly sophisticated narrow band tunable laser systems had to be developed. Narrow band lasers resonant with14CO2transitions provide the required specificity, but greatly enhanced sensitivity to small numbers of resonant atoms is also required. SCAR achieves enhanced sensitivity through the cavity ringdown effect obtaining effective path lengths of order 10km. ICOGS also achieves similar enhancement by placing the sample inside a laser cavity

achieving effective path lengths of the order of 50 km. The ICOGS sensitivity is further enhanced by the optogalvanic effect[3]. Laser radiation changes the distribution of various species molecular level populations within an electrical discharge, which in turn changes the electron energy distribution function. This leads to an easily measurable impedance change of the system.

0.2.1 Optogalvanic Effect

The basic concept of OGE detection has long been used in atomic and molecular spectroscopy. If a laser of intensity I, and frequency v is incident on a cylindrical (length L3 and radius R) weak electrical discharge, the electrical response, S, of the discharge can be expressed by an integral over the laser-discharge interaction volume:

$$S = \int_0^L dz \int_0^R r dr \int_0^{2\pi} d\theta [n(r,\theta,z) I(r,\theta,z,\nu) \sigma(\nu) K] \qquad (1)$$

where *n* is the density of interacting species and $\sigma(v)$ refers to the laser-species interaction cross section. *S* can be any discharge parameter related to conductivity and K is a corresponding optogalvanic proportionality constant that depends on the details of the electrical discharge. If more than one group of molecules interacts with the laser,as discussed below, the signal then becomes a sum over all interacting species. A good approximation of the OGE signal is:

$$S(\nu) = n L_{eff} I A \sigma(\nu) K \qquad (2)$$

Here, *n* represents the average molecular density of interacting particles, *Leff* the effective length of the interaction region, *I* the average laser intensity and *A* the

average area of the laser beam. As implied by the equation, detection of trace amounts of molecules,such as contemporary or sub-contemporary levels of 14*CO*2 requires high laser intensity, maximinteraction cross sections, large *Leff* and optimum discharge conditions to enhance the population of the interacting species as well as the magnitude of the optogalvanic proportionality constant. Previous work [19, 18, 17] have shown how 13*C* isotopic abundance can be determined in small samples with high precision in an external discharge cell with *Leff* enhanced over the discharge length by back reflection of the incident laser beam. For 14*C* analysis, *Leff* must be enhanced by many orders of magnitude, and the analyte cell is now placed inside the laser cavity, providing high circulating laser power as well as the required *Leff*. The simplicity of equation (1) and (2) mask a deeper complexity. The experimentally 4 measured *S* is really the difference between a baseline impedance ($I = 0$) and *S* at intensity *I* with the laser chopped on and off at a frequency *f*; introducing a time dependence. The greatly enhanced sensitivity also amplifies background effects and the interacting species density *n* can be considered to consist of three different entities: *n*1, the background buffer gas (typically nitrogen), *n*2, the more abundant *CO*2 isotopes and *n*3, the resonant 14*CO*2 species. Each species has a different interaction cross section σi and possibly a different *Ki*. *Ki* can also have different time dependencies. *Leff* which can reach several hundred km is limited by $c\Delta tL/Lc$, for all species, where c is the speed of light, Δt is the time of observation or half the chopping period, *L* the cell length and *Lc* the laser cavity length. In external cavity experiments, such as SCAR, a similar *Leff* is determined by the quality of

the cavity used and is as large as 10km. Though similar in many respects to the well-studied and highly sensitive intracavity absorption spectroscopy (ICAS)[2], ICOGS is fundamentally different, and even more sensitive. SCAR is more similar to ICAS as the absorption of light via the change in intensity of a laser beam is measured, in one case by the time decay of light exiting the cavity, in the other by the change in laser intensity due to internal absorption. In contradistinction to ICAS or SCAR, ICOGS measures the electrical effect due to energy lost (absorption), or gained (stimulated emission), by the laser beam in the intracavity discharge cell that can be considered to be a highly sensitive calorimeter. ICAS is most sensitive for tunable multimode lasers where the intracavity absorption affects the laser mode competition leading to a change in the laser output as a function of wavelength. Theory [12] correctly predicts that such changes for single mode lasers such as the *CO*2 lasers used in these studies should be absent, except near laser threshold, due to gain saturation in the lasing medium compensating for the small absorption loss in the intracavity cell. Surprisingly large and highly non-linear ICAS results were recently reported, however, using a single mode *CO*2 laser[7]. These results can be attributed 5 to the frequency pulling effects due to the very high density of narrow band absorption present. In the experiments reported here, however, the laser intensity variation due to changes in the intracavity laser cell is not measurable and assumed to be zero in agreement with ICAS theory. In addition, the ICOGS cell can be considered to be a tiny part of the total saturated laser gain system. According to equation (2), the total measured ICOGS signal *SOG* can be

expressed as a sum of three terms:

$$S_{OG} = S_{bgd} + S_{off\_resonance} + S_{^{14}CO_2} \quad (3)$$

where *Sbgd* is the non resonant background signal due to the buffer gas, *Soff_resonance* is the signal due to the wings of transitions in 12,13*CO*2 and *S*14*CO*2 is the on resonance signal due to radiocarbon. All three terms are subject to the same huge *Leff* and high internal laser power, up to 40W in our case, however they differ in three significant ways. First, the interacting densities are vastly different, as are the interaction cross sections, with the high resonant laser cross section for 14*CO*2 compensating for its low concentration in contemporary *CO*2. Second, the optogalvanic coupling coefficients, *Kx*, differ for the background nitrogen compared to the *CO*2 present. Third, the three signal components can have differing signs because the optogalvanic effect can be either positive or negative depending on how the impedance change is affected[24]. In absorption spectroscopy, a continuously tunable laser is used and the various contributions to a signal are determined from fitted line shapes and known absorption cross-sections to determine one or more unknown parameters such as densities. Further, the absorption spectrum is almost always based on transitions the ground state. The ringdown spectroscopy absorption spectroscopy work for 14*CO*2 could only be carried out due to technological advances in continuously tunable extremely narrow band lasers over a relatively large band width. The work herein reported, however, could have been carried out more than 20 years ago with the then existing extremely narrow band fixed frequency isotopic *CO*2 lasers. As previously mentioned the basic physics of

ICOGS was studied in connection with *CO*2 laser and optogalvanic effect physics in the 1970s and 80s. ICOGS, like all OGE spectroscopy involves the use of gas discharges, allowing access to non-ground state transitions. In fact, if the analyte gas mixture is chosen correctly greatly enhanced populations of the resonantly interacting species can be obtained by the same collisional exchange mechanism that makes the *CO*2 laser so efficient. And, since the analyte cell is so similar to the laser gain medium the extensive literature on modeling the *CO*2 laser can be employed. The laser interaction of the *CO*2 in a glow discharge of *N*2 with *CO*2 taking place in an optogalvanic cell can be modeled as a simple gain medium. The equation for the gain of the cell, *g*, is given by:

$$\begin{aligned} g(\nu, r, t, I) &= \sigma(\nu)(N_u^J(\nu, r) - N_l^{J+1}(\nu, r)) \\ &= G_0 N_{total}(r, t) f(I(r), \nu) \end{aligned} \tag{4}$$

The optogalvanic respose, however. is proportional to the energy gained or lost in the cell, ΔE, and is given by:

$$\Delta E = 2\pi L_{eff} \int (g_{14} + g_B) I(r) r dr \tag{5}$$

Here *I* represents the internal laser intensity, *σ* represents the absorption cross section, Nu represents the upper laser level, and *Nl* represents the lower laser level populations present. *G*0 is the unsaturated gain in the cell and *f* represents a saturation function (discussed below). The parameter *g*14 is the resonant gain and *gB* is the loss summing over the Lorentzian tails from all other contributing non resonant transitions. Because the laser is essentially CW and the absorber

density is too low to change the intracavity laser power, the intensity is a time independent parameter chopped from 0 to *I* at a (low) frequency *f*. The molecular transition rates are orders of magnitude faster than the transport of the molecules, so the measured dependence on f is determined by diffusion of the *CO*2 in the sample cell into and out of the laser beam [23] relative to the chopping period. In figure 1, we show the expected time dependence of the signal calculated with this model and data obtained by varying the chopping frequency.

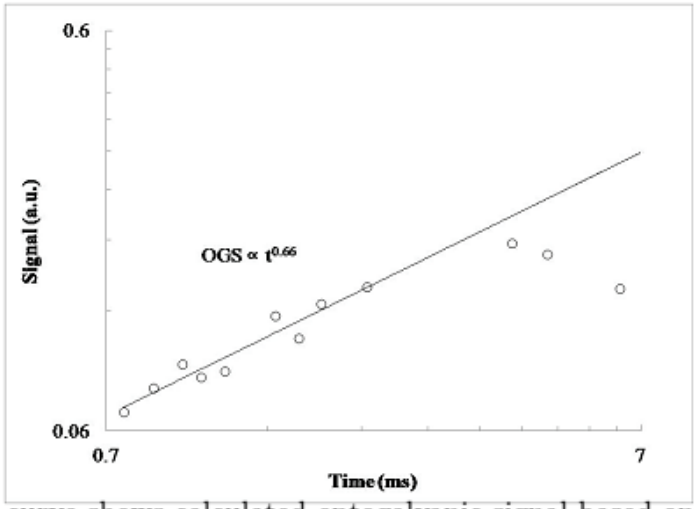

Fig. 1: The solid curve shows calculated optogalvanic signal based on CO_2 diffusion in the ICOGS cell (solid curve). The points are measurements as a function of chopping period scaled to the calculations at long times.

Both the on- and off-resonance CO2 contributions to *S* are estimated to be of comparable size under typical experimental conditions. Although the major interacting transitions in the 13,12*C*17,18*O*2 molecules are off resonance by several thousand natural linewidths, the densities of 13,12*C*17,18*O*2 in most *CO*2 samples can be up to 1014 larger then those of 14*CO*2. The resonance of the 14*CO*2 in the sample with the 14*CO*2 laser transitions leads to power

saturation in *S*14*CO*2 which is not the case for *Soff_resonance*. The onand off-resonance species also differ with respect to their rotational quantum numbers, J. The closest possibly contributing transitions for 13,12*CO*2 are from high J states (68) and these transitions are slower than J(21) transition of 14*CO*2.[10] Because the relevant transitions here are very far off resonance, their total loss, *gB* can is given by a sum over all contributing transitions:

$$g_B(\nu) = \sum G_0^B L(\Delta\nu) \tag{6}$$

where *GB*0 is the small signal gain and *L*(Δ*v*) represents the Lorentzian evaluated at the laser resonance which is very far from line center. The sum is evaluated over all the relevant contributions from the closest laser transitions for 13,12*CO*2. It should be emphasized that, when *CO*2 is the minority species in a nitrogen buffer gas, the excited state population densities outside of the rotational states within a given vibrational state cannot be calculated using simple Boltzmann factors. This is due to the collisional excitation of the upper CO2 laser levels that leads to population inversion [21]. Also, some allowed transitions can have low optogalvanic response. Experimentally, the total contribution from the non-resonant *CO*2 contributions can be determined, as shown below, by comparison with measurements of radiocarbon-free *CO*2. Background and resonant molecules also saturate differently and have different line shapes. In the sample cell, both Doppler broadening and Lorentzian broadening are important, as are velocitychanging collisions and rotational relaxation rates. This situation was carefully studied in the 1970s [9]. As the 14*CO*2 P(20) laser line is extremely far from any known nitrogen resonance, the

Sbgd component that comes from the buffer gas can be attributed to transitions near the ionization continuum, where population densities are very low but the OGE factor K can be large. This hypothesis is consistent with the rapid decrease in intensity experimentally observed in *Sbgd* with increasing pressure, where increased collision rates with increased pressure quench the high lying states. This hypothesis also explains the observed difference (discussed below) between the time dependence of the *Sbgd* with respect to the laser chopping, compared to that of *Soff* resonance and *S*14*CO*2. The nitrogen background signal is easily measured and discussed in previous papers [19, 18, 17]. We have previously observed that a 20:1 nitrogen *CO*2 mixture at a pressure near 5 torr greatly enhances the *KCO*2 for the resonant transitions and that *K* becomes non-linear when the *CO*2 concentration is much greater than a few percent. Accordingly, we have kept the maximum concentrations of *CO*2 in *N*2 below 5% in our experiments. This is the same reason that a *CO*2 laser has *CO*2 as the minority species for maximum gain. Helium is the majority gas in the laser gas medium for cooling and collisional quenching of the lower laser level. It is a poor buffer for the sample cell, however, as it greatly reduces the optogalvanic effect[26]. Also, due to pressure broadening of the *CO*2 off-resonance contributions to *SICOGS*, lower pressure is favored; generally, a pressure between 0.8 to 1.0 torr has been used in our experiments. The *N*2 - *CO*2 discharge studied here is different from that of 100% CO2 discharge that was also studied in our earlier work[8] in three significant ways. First, the background for excitation near the continuum cannot obviously be

separated from the off resonance transitions by experiment. Secondly the optogalavanic response is likely different for the low lying off resonance transitions compared to the background near the continuum. Third, and most importantly, the populations of various states are expected to be proportional to their Boltzmann factors and show different laser saturation behavior when compared to the collisonally enhanced laser level populations of *CO*2 in a nitrogen buffer. In our first publication, we showed data obtained with the P(20) line in 100% *CO*2 that yielded a much larger signal than could be obtained with the nearby P(18) and P(22) lines. The 14*C* contribution to the observed signal was small, but measurable.

This is now attributed to an accidental near resonance of the P(20) 14*CO*2 transition with a weak transition in 12*CO*2 having a large optogalvanic proportionality constant. In this case, the separation of the 14*CO*2 signal from the total signal could only be accomplished empirically by plotting average double ratios against the known 14*C* concentration of calibration samples. Only a small, easily saturated fraction of the overall signal was attributed to the resonant 14*CO*2 transitions, but this fraction was observed with a high signal to noise ratio using relatively long averaging times. Not surprisingly, this situation is extremely sensitive to discharge conditions and requires frequent recalibration. In this paper, we concentrate on the more theoretically tractable situation of practical importance that of small samples in nitrogen buffer gas. We note, however, that the pure *CO*2 system may be useful for many monitoring situations[11] where large samples are available and the

dynamic range of interest is limited. As indicated above the non-linear multi-parameter dependence of *SICOGS* can make instrumentation calibration challenging. ICOGS cannot be an absolute measurement system for 14*CO*2, but, as is typical for laboratory analytical instruments, it must rely on well-characterized standards for calibration. The relative simplicity, compactness and ease of use, however, may make ICOGS ideal for a laboratory instrument for many applications including carbon dating, environmental monitoring and biological tracer work.

0.3 ICOGS OG Signal Analysis

In this section, we simulate our ICOGS OG signals of *CO*2 based on a two-level rate equation and *N*2 based on a set of 4-level rate equation.

0.3.1 *CO*2 OG Signal Simulation

When the laser beam is incident on the gas medium, the vibrational energy distribution at relevant vibrational states is modified due to the absorption or induced emission of the photons. This causes a change of the sample cell conductivity and the OG signal *S* can be detected. The temporal variation of the population densities and total kinetic energy ε in the (001) and (100) levels (figure 2), *M*1, *M*2 and ε, is described by the following rate equations [22],[24]:

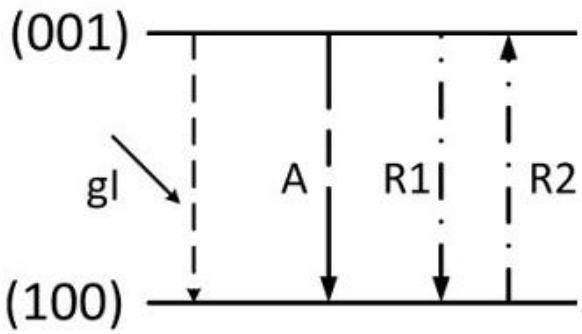

Fig. 2: CO_2 OG signal simulation rate equation structure

$$dM_1/dt = -(R_1 + A)(M_1 - M_1^*) - gI(M_1 - M_2) \quad (7)$$

$$dM_2/dt = -R_2(M_2 - M_2^*) + gI(M_1 - M_2) \quad (8)$$

$$d\varepsilon/dt = R_1E_1M_1 + R_2E_2M_2 - R(\varepsilon - \varepsilon^*) \quad (9)$$

Where the definitions of the symbols used in equations above are summarized in table 1. Figure 3 shows our simulated *CO*2 OG signal (red line) compared with our experimental result (blue line) and Figure 4 shows the positive and negative OG signal simulation under different pressure environments.

Symbol	**Definition**	**Value**
A	Spontaneous emission rate	385 Hz
g	Induced emission rate	948Hz//W
M_1^*, M_2^*	Non-perturbed population density of M_1, M_2	$M_2^*/M_1^* = 0.024$
R_1, R_2	Vibration-transition relaxation rates of (001),(100)	R_1= 70 Hz/Torr R_2= 1700 Hz/Torr
R	Kinetic energy relaxation rate	15921 Hz/P

Table 1: List of parameters in rate equation

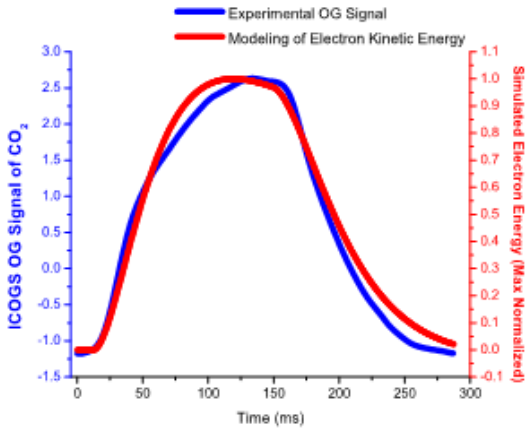

Fig. 3: CO_2 OG signal. Experiment and Simulation

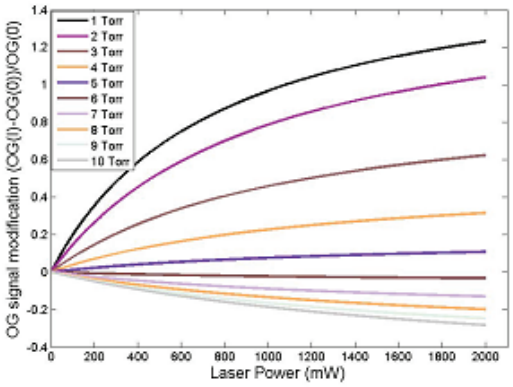

Fig. 4: CO_2 OG signal simulation under different conditions

0.3.2 *N*2 OG Signal Simulation

As the 14*CO*2 P(20) line laser frequencies are extremely far from any known nitrogen resonance, we do not have *N*2 OG signals for *N*2 buffer gas. However, in our ICOGS system, within which we have an internal sample cell, the *Sbgd* component from *N*2 buffer gas become our main background signal. From Equation 3, this signal can be attributed to transitions near the ionization

continuum, where population densities are very low but the OGE factor *K* can be large. Thus, in this paper, a four-level rate equation (Figure 5, considering *N*2 ground state, meta-stable state[5], highly excited state and excited state, is proposed to simulate *N*2 OG signal. The *N*2 OG signal computed from

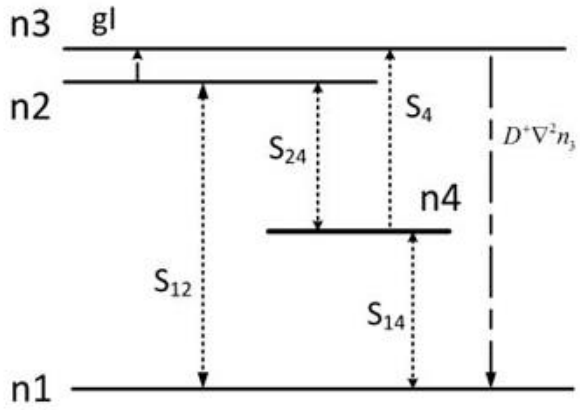

Fig. 5: N_2 OG signal simulation rate equation structure

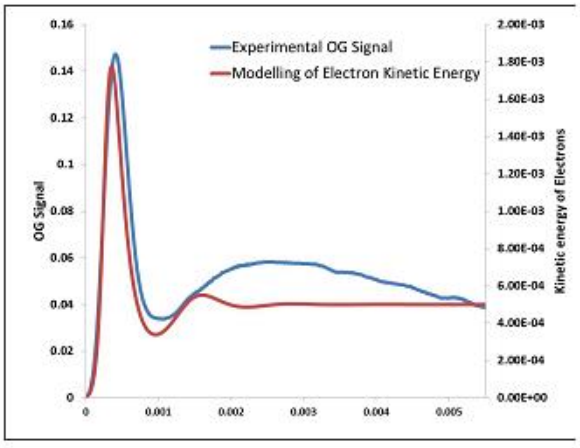

Fig. 6: N_2 OG signal. Experiment and Simulation

our 4 level rate equation model agrees best with our ICOGS *N*2 OG signal, however, the slow component starting from 2ms is probably due to two reasons: 1. more energy transmissions are allowed and a more comprehensive rate equation is needed to simulate *N*2 OG signal; 2. incident laser has a thermal

effect on the sample cell(Figure 6).

0.4 Signal Separation and Analysis

It is crucial to separate the slow *CO*2 OG signal component from the fast *N*2 OG signal. Here in this section, we propose three ICOGS OG signal separation methods: (1)Vector Phase and Amplitude fitting; (2)Differential Method; (3) Vector Decomposition Method.

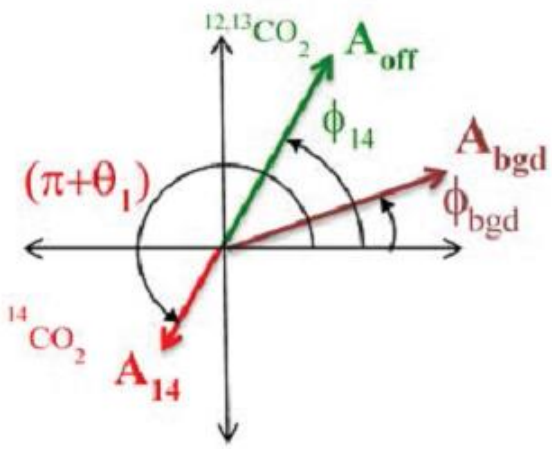

Fig. 7: Vector representation of OG signal components

0.4.1 Vector Phase and Amplitude fitting

As the ICOGS OG signal of *CO*2 and *N*2 have a very different phase response to the incident laser, it is possible to separate these signals by Fourier Analysis. By taking the fourier transformation fundamental component of the coherent wave, we define the total OG signal as the following three components (also see figure 7):

$$\frac{FT(S_{total}^{sam})}{FT(S_{total}^{ref})} = A_{bgd}e^{i\phi_0} + A_{off}Ke^{i\phi_{off}} + A_{14}Ke^{i\phi_{14}} \tag{10}$$

where the first term on RHS is the *N*2 buffer gas OG signal, the second term is off resonant 12,13*CO*2 component and the third term is on resonant 14*CO*2 component. *K* is defined as percentage of *CO*2 in our sample cell. Here, we make the following assumptions:

1. A_{bgd} does not depend on the concentration of CO_2
2. A_{off}, A_{14} are linearly depend on the concentration of CO_2, K
3. ϕ_{off} and ϕ_{14} have a π phase difference

By fitting the measured total amplitude *At* to the percentage of *CO*2 *K* from experimental data to the following expressions, we can obtain *A*14 which indicates 14*CO*2 concentration.

$$A_t = \sqrt{(A_{bgd}cos(\phi_{bgd}))^2 + (K(A_{14} - A_{off})cos(\phi_{14}))^2} \tag{11}$$

$$tan(\phi_t) = \frac{K(A_{14} - A_{off})tan(\phi_{14}) + A_{bgd}tan(\phi_{bgd})}{K(A_{14} - A_{off})cot(\phi_{14}) + A_{bgd}cot(\phi_{bgd})} \tag{12}$$

0.4.2 Differential Method

Another analysis method which can get a high fitting quality is the differential method. In general, the coherent wave of a single period OG signal has three components:

$$C_{total}(t; K, M) = C_{N_2}(t; K) + C^{12}(t; K) + C^{14}(t; K, M) \tag{13}$$

where *Ctotal*is the total OG signal which has three components: *CN*2 due to the Nitrogen buffer gas, *C*12 12*CO*2 and *C*14 14*CO*2 component.Define the time

average of function *f*(*t*), we can obtain the change of OG signal from time *t* + 1 to *t* (where the time is taken as one second average) as:

$$\begin{aligned}&\Delta C_{total}(t;K,M)\\&=\frac{\partial(C_{N_2}(t;K)+^{12}\overline{C}(t;K)+^{14}\overline{C}(t;K,M))}{\partial K}\Delta K\end{aligned}\tag{14}$$

Instead of the strong assumption in vector decomposition method, we assumes:

1. if the change of K is very small between adjacent coherent waves, the change of *N*2 signal is neglected: *∂CN ∂K* 2(*t*;*K*) ≈ 0

2. OG signal phase dependent component (*ϕ*(*t*)) and sample gas density demendent component (*f*(*K*)) are dissociable:

12*CO*2(*t*; *K*) = *ϕ*12(*t*)*f* 12(*K*)

14*CO*2(*t*; *K*) = *ϕ*14(*t*)*f* 14(*K*)

When inject sample gas of pure 12,13*CO*2 (dead sample), in which case (14*C*)signal is zero, we can get:

$$\Delta\overline{C}_{total}(t,K,M=0)=\overline{\phi}^{12}(t)\frac{\partial f^{12}(K)}{\partial K}\Delta K$$

By fitting Δ*Ctotal* -Δ*K*, we can get a linear fit with a slop *slopedead* and 0 intercept:

$$\overline{\phi}^{12}(t)\frac{\partial f^{12}(K)}{\partial K}=slope_{dead}\tag{15}$$

since both the phase average *ϕ*12(*t*) and the *slopedead* are constant, we can rewrite *f* 12(*K*) as *AoffK*. In other words, from *slopedead* we can get the information representing the *Aoff* component: *ϕ*12(*t*)*Aoff* = *slopedead* from

sample with 14*CO*2 gas mixed, we fit $\Delta Ctotal$ - ΔK and get a linear fit with a slope *slopemodern* and an 0 intercept which is：

$$\bar{\phi}^{12}(t)\frac{\partial f^{12}(K)}{\partial K} + \bar{\phi}^{14}(t)\frac{\partial f^{14}(K)}{\partial K} = slope_{modern} \quad (16)$$

From equation (16) we can get the information representing *A*14 component:

$$\bar{\phi}^{14}A_{14} = (slope_{modern} - slope_{dead})$$

0.4.3 Vector Decomposition Method

The Vector Decomposition Method is built based on our Vector Phase and Amplitude Fitting method. Instead of fitting the complex equations (12) and (13), we first calculate subtracted vector *Atotal−Abgd*, which is supposed to be a constant phase (*ϕ*14) vector with varying amplitude (*K*). Thus, only a linear fit is necessary to calculate *A*14 information:

$$\sqrt{(A_{total}sin(\phi_t) - A_{off}Ksin(\phi_{off}))^2 + (A_{total}cos(\phi_t) - A_{off}Kcos(\phi_{off}))^2} = A_{14}K \quad (17)$$

0.5 Experiment

The architecture and facilities of a prototype ultra-sensitive ICOGS system are shown in Figure 8. Determining *S*14*CO*2 from the measured *SICOGS* is straightforward. Concurrent with the ICOGS signal, a single pass OG signal for 12*CO*2 is measured transverse to the 14*CO*2 laser axis for normalization of the *S*14*CO*2 to total carbon content. *Sbgd* is determined by measuring the *SICOGS* of the buffer gas in the absence of *CO*2, and the *Soff−resonance* is determined using a “dead” *CO*2 sample. The desired 14*CO*2 calibration curve is obtained by

measuring the *SICOGS* of a series of standards with known 14*CO*2 levels. Because all the signals are dependent on laser power and wavelength, an external reference cell is employed to concurrently determine the OGE for a 14*C* enriched *CO*2 in nitrogen sample. The *SICOGS* signals from the reference cell are used to stabilize the wavelength line centers, and also to calculate the ratio of the sample to reference signals, minimizing the noise coming from fluctuations in the laser power and the glow discharge.

A major feature of ICOGS is that relatively small samples can be used and sample introduction *CO*2 into a buffer gas, typically nitrogen is straightforward. Prototype systems anticipate coupling of separation devices (LC with oxidation or GC) to an analytical instrument with simultaneous monitoring of the *CO*2 concentration and *SICOGS* to determine 14*C* concentration. In the current prototype system, approximately 10 micromoles *CO*2 are typically injected into the flowing buffer gas which feeds into a stable discharge. The pressure and flow rate are controlled to maintain a constant pressure near 1 torr with less than 5% *CO*2 concentration. As in previously reported designs, the ICOGS signals are taken from analysis of the variation in RF amplitude driving the glow discharge that occurs in phase with the laser chopping frequency. Cross-talk between the laser pulses is minimized by the use of prime-number chopping frequencies. As a result, the 12*CO*2 and 14*CO*2 lasers can excite both the sample and reference cells simultaneously to generate four concurrent signals 12*C* sample, 12*C* reference, 14*C* sample, and 14*C* reference which produce two independent (sample / reference) ratios, the 14*C* ratio and the 12*C* ratio. In previous studies,

we only used the real component of the signal magnitude to estimate the fraction of 14*C*. In this study, we take into account the real and imaginary components of the response (the amplitude and phase). An example of this analysis is shown in Figure 9.

Figure 9(a) shows 12*C* signal produced by a 100 *μgm* sample as it flows in and out of system with nitrogen buffer at 1 torr. 9(b) shows the 14*C* ratio amplitude and phase signals being measured concurrently.

To compute *A*14 from equation 11, these four parameters (*Abgd*,*ϕbgd*, *Aoff* and *ϕ*14) should be pre-determined. In experiment, we first determine *Abgd* and *ϕbgd* from the pure Nitrogen buffer gas range (0∼20 minutes in figure 10, where no *CO*2 is present. Then, *ϕ*14 is determined by fitting equation 12 to the data taken from range 26∼80 minutes where pure 12,13*CO*2 is flowing through our sample cell. Finally, *Aoff* is taken as the fitting parameter from 11. The reason why we use equation 12 to determine *ϕoff* is that the phase parameter is most sensitive to *ϕtotal* and thus a more precise *ϕoff* is determined.

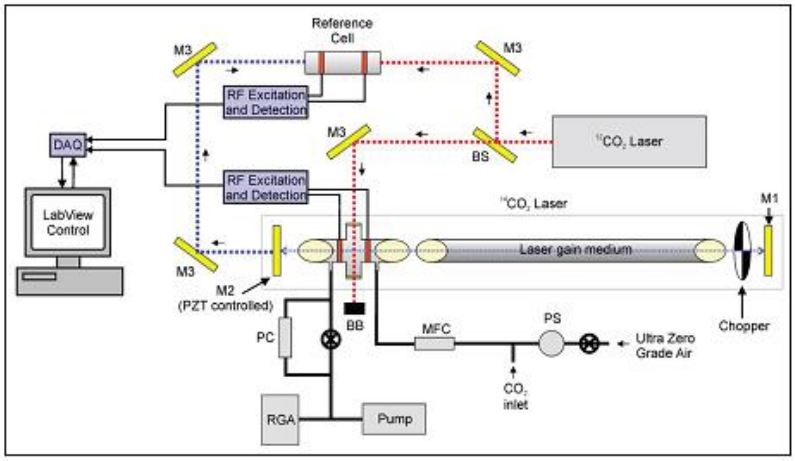

(a) ICOGS System Architecture

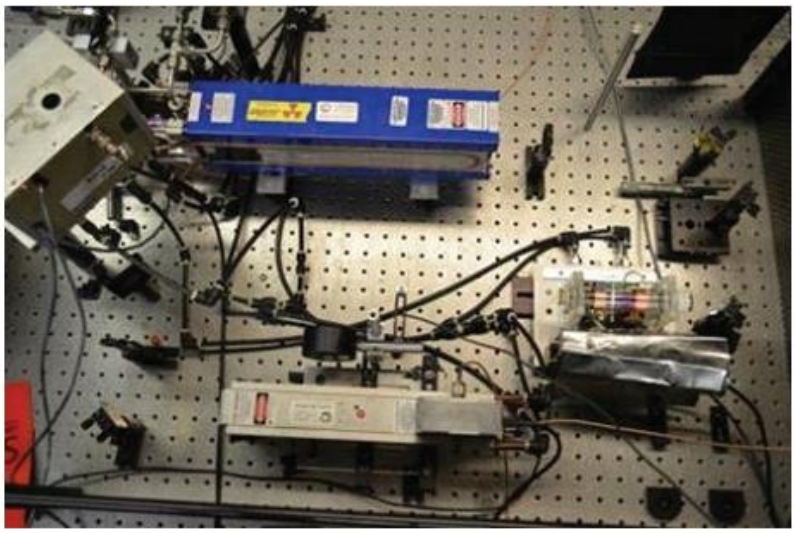

(b) ICOGS Experiment Facilities

Fig. 8: ICOGS System Architecture and Experiment Facilities Presentation

The *A*14 from different standard samples is determined from the 4 injections of sample gas with different 14*CO*2 content mixed, with the similar fitting progress of determining *Aoff* mentioned above. In this manner, a calibration curve of *A*14 can be determined using a series of standards, as shown in Figure 11. In Figure 11, the point plotted near 10−4 Modern is taken as the measured value for “dead” *CO*2 and used for calculation of the *Aoff* resonance component. This

concentration can be considered an approximate limit of detection (LOD) for the ICOGS measurement and is similar to the LOD of $\sim< 10{-}15$ for most AMS systems. Due to saturation effects, decreased laser power leads to better separation at higher 14*C* enrichments - an important consideration for designing smaller size and lower cost instrumentation for highly 14*C* enriched labeled compound studies. Conversely, an increased laser power allows for a lower limit of detection (LOD). Quantitative experiments to obtain a lower LOD by dilution studies with high power are in progress. The calibration is dependent on pressure as well as discharge conditions and is best represented by a power law (red line). The power law is related to the well-studied energy model for the OGE in *CO*2 gain discharges[26, 15]. In our case, the measured OGE is proportional, to the change in RF voltage in the discharge cell, whereas it is the total energy deposited that should be linear in 14*CO*2 concentration. The relationship of energy deposited to voltage change in an rf discharge is complicated, and can be positive or negative depending on pressure and gas composition[26].

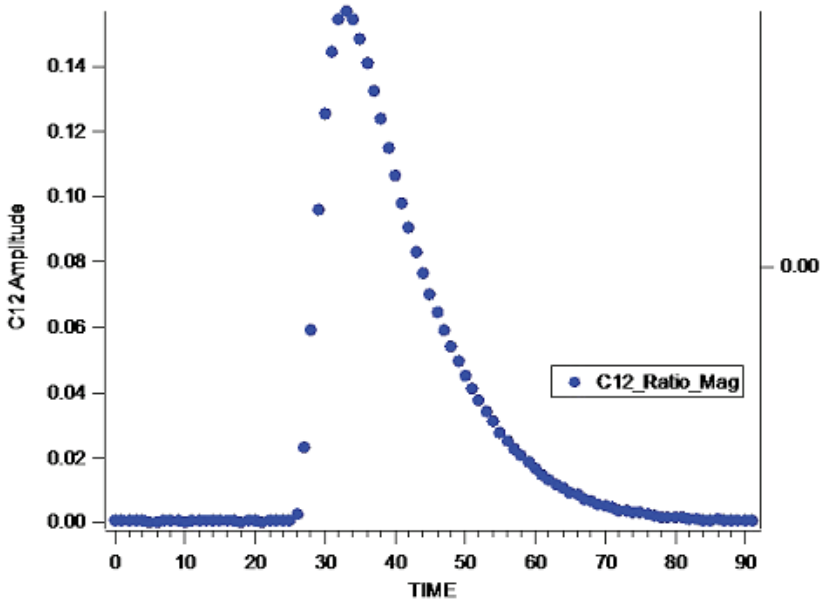

(a) ^{12}C signal as sample gas flows through OG cell

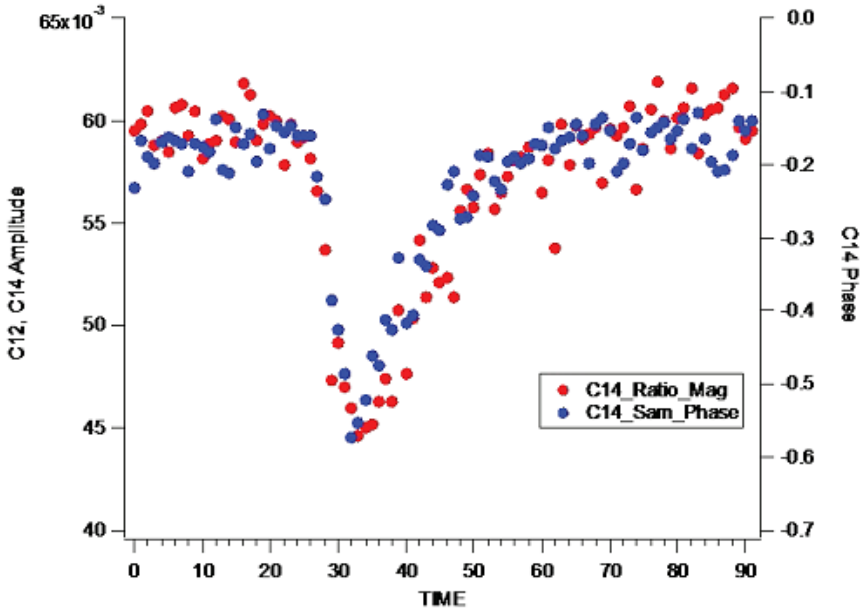

(b) ^{14}C signal as sample gas flows through OG cell

Fig. 9: Experimental Signals Collection and Presentation

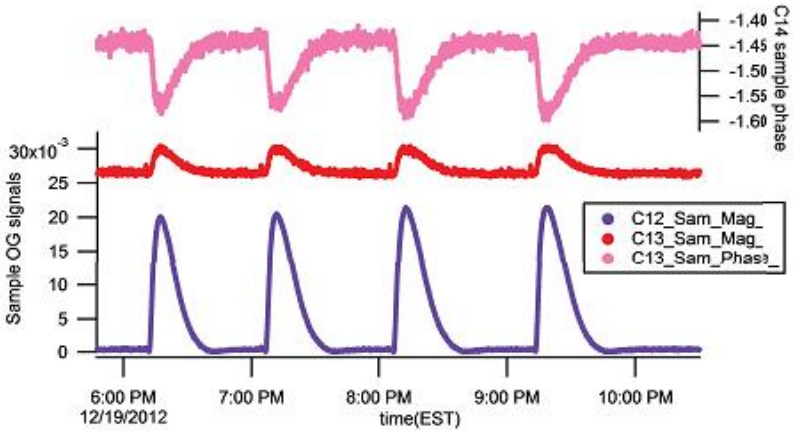

Fig. 10: Experimental signals of four standard $^{14}CO_2$ mixed sample gas flowing throu sample cell in succession.

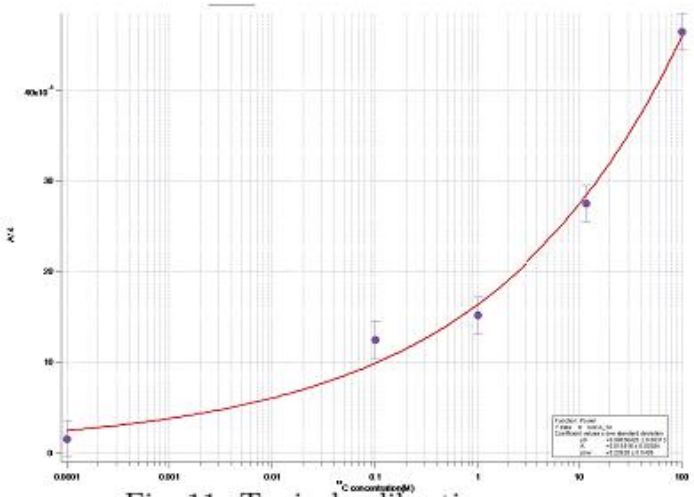

Fig. 11: Typical calibration curve.

0.6 Summary and Outlook

In previous reports, ICOGS has been demonstrated as an effective technique for radiocarbon detection over several orders of magnitude above and below contemporary concentrations of 14*C*. The ICOGS theory presented here is general, and though the case for carbon isotopes is particularly attractive, similar laser-based instrumentation could be developed for other trace gas detection applications. It is based on the compact, scientific *CO*2 laser: a mature

technology with modest cost that although filled with a 14*CO*2 laser gas mix, emits no detectable radioactivity. As a sealed source, it can be shipped without special precautions under US, Canadian and EU radioactive source regulations. Even if the gas mix should leak, there is no radiologic health risk from the small amounts of radiocarbon which has a very short biological half-life and is rapidly diluted in the atmosphere in any case. The precision and accuracy possible with ICOGS are comparable and even superior to AMS machines, using only sample sizes in the 100 microgram and lower size range. This sensitivity is attainable because the precision of the ICOGS measurement is based on the averaging time and the signal to noise ratio, rather than counting statistics. Implementation of continuous automated measurement of multiple samples is also possible, which would constitute an important development for the efficient analysis of 14*C*-labeled compounds and similar studies. Precision at 1% to levels with as low as 10−14 concentration is expected with even better results within limited dynamic ranges. When the measurement spans over 3 orders of magnitude near contemporary levels, as is necessary for tracer studies, 5% precision is achieved with a few minutes measuring time per sample. Engineering of a user friendly ICOGS system, similar to a 13*C* breath testing instrument based on the OGE effect[6] presents no fundamental problems. Major technical areas for improvement include replacing the analog OGE detector with more modern digital electronics and higher quality pressure and temperature stabilization. Initial improvements have shown precision at the 0.5 per mil level.

Bibliography

[1] G. Alimonti, G. Angloher, C. Arpesella, M. Balata, G. Bellini, J. Benziger, S. Bonetti, L. Cadonati, F.P. Calaprice, G. Cecchet, M. Chen, N. Darnton, A. de Bari, M. Deutsch, F. Elisei, F. von Feilitzsch, C. Galbiati, F. Gatti, M.G. Giammarchi, D. Giugni, T. Goldbrunner, A. Golubchikov, A. Goretti, T. Hagner, F.X. Hartmann, R. von Hentig, G. Heusser, A. Ianni, J. Jochum, M. Johnson, M. Laubenstein, P. Lombardi, S. Magni, S. Malvezzi, I. Manno, G. Manuzio, F. Masetti, U. Mazzucato, E. Meroni, M. Neff, A. Nostro, L. Oberauer, A. Perotti, A. Preda, R.S. Raghavan, G. Ranucci, E. Resconi, M. Ruscitti, R. Scardaoni, S. Sch?nert, O. Smirnov, R. Tartaglia, G. Testera, P. Ullucci, R.B. Vogelaar, S. Vitale, and O. Zaimidoroga. Measurement of the 14c abundance in a low-background liquid scintillator. *Physics Letters B*, 422(1¨C4):349 – 358, 1998.

[2] H Atmanspacher, H Scheingraber, and CR Vidal. Dynamics of laser intracavity absorption. *Physical Review A*, 32(1):254, 1985.

[3] Beniamino Barbieri, Nicolo Beverini, and Antonio Sasso. Optogalvanic spectroscopy. *Reviews of modern physics*, 62(3):603, 1990.

[4] N Barnes, S Benson, F Duarte, C Freed, D Harris, R Sze, and P Zorabedian. Tunable lasers handbook, 1995.

[5] G Cernogora, L Hochard, M Touzeau, and C Matos Ferreira. Population of n2 (a3σu+) metastable states in a pure nitrogen glow discharge. *Journal of Physics B:*
Atomic and Molecular Physics, 14(16):2977, 1981.

[6] Van Der Hulst et al. Laser assisted ratio analyser 13c-urea breath testing, for the detection of h. pylori: a prospective diagnostic european multicentre study. *Alimentary pharmacology & therapeutics*, 13(9):1171–1177, 1999.

[7] Mohammad Eskef and Sharif Al-Hawat. Modeling of the power oscillation observed in single mode intracavity absorption of co 2 laser lines. *Optics & Laser Technology*, 43(8):1431–1435, 2011.

[8] I Galli, S Bartalini, S Borri, P Cancio, D Mazzotti, P De Natale, and G Giusfredi. Molecular gas sensing below parts per trillion: radiocarbon-dioxide optical detection. *Physical review letters*, 107(27):270802, 2011.

[9] J Goela and TF Morse. Saturation effects and lamb-dip formation in molecular lasers. *Quantum Electronics, IEEE Journal of*, 12(5):281–290, 1976.

[10] JS Goela and TF Morse. Increased inversion efficiency in optically pumped twolevel molecular systems. *Optics letters*, 4(11):375–377, 1979.

[11] KM Hämäläinen, H Jungner, O Antson, J Räsänen, K Tormonen, and J Roine. Measurement of biocarbon in flue gases using 14c. *Radiocarbon*, 49(2):325–330, 2007.

[12] H Kimble. Calculated enhancement for intracavity spectroscopy with a single-mode laser. *Quantum Electronics, IEEE Journal of*, 16(4):455–461, 1980.

[13] Graham Lappin and R. Colin Garner. Big physics, small doses: the use of ams and pet in human microdosing of development drugs. *Nature Reviews Drug Discovery*, 2:233–240, 2003.

[14] Beer-Lambert Law. Cavity-ringdown spectroscopy–an ultratrace-absorption

measurement technique. 1999.
[15] S Moffatt and ALS Smith. Temperature perturbation model of the opto-galvanic effect in co2 laser discharges. *Journal of Physics D: Applied Physics*, 17(1):59, 1984.
[16] Daniel E Murnick, Ozgur Dogru, and Erhan Ilkmen. Intracavity optogalvanic spectroscopy. an analytical technique for 14c analysis with subattomole sensitivity. *Analytical chemistry*, 80(13):4820–4824, 2008.
[17] Daniel E Murnick and Joseph O Okil. Use of the optogalvanic effect (oge) for isotope ratio spectrometry of 13co2 and 14co2. *Isotopes in Environ Health Studies*, 41(4):363–371, 2005.
[18] DE Murnick, MJ Colgan, and DJ Stonebach. Laser optogalvanic isotope ratio analysis in carbon dioxide. *Synthesis and Applications of Isotopicaly Labeled Compounds*, page 111, 1997.
[19] DE Murnick and BJ Peer. Laser-based analysis of carbon isotope ratios. *Science*, 263(5149):945–947, 1994.
[20] Ted J. Ognibene, Graham Bench, John S. Vogel, Graham F. Peaslee, and Steve Murov. A high-throughput method for the conversion of co2 obtained from biochemical samples to graphite in septa-sealed vials for quantification of 14c via accelerator mass spectrometry. *Analytical Chemistry*, 75(9):2192–2196, 2003. PMID: 12720362.
[21] CKN Patel. Selective excitation through vibrational energy transfer and optical maser action in n 2-c o 2. *Physical Review Letters*, 13(21):617, 1964.
[22] David M Pepper. Analysis of the optogalvanic effect in discharge plasmas using rate equations in a modified schottky formalism. *Quantum Electronics, IEEE Journal of*, 14(12):971–977, 1978.